Journal of Solid State Chemistry **155,** 259–272 (2000)
doi:10.1006/jssc.2000.8962, available online at http://www.idealibrary.com on IDEAL®

Symmetry-Breaking Transitions from $GdCuAs_2$ through $GdCuAs_{1.15}P_{0.85}$ to $GdCuP_{2.20}$: Crystal Structure, Application of Landau Theory, Bonding, Magnetic and Electrical Properties

Yurij Mozharivskyj,* Dariusz Kaczorowski,† and Hugo F. Franzen*,[1]

*Department of Chemistry and Ames Laboratory of US DOE, Spedding Hall, Iowa State University, Ames, Iowa 50011; and
†W. Trzebiatowski Institute of Low Temperature and Structure Research, Polish Academy of Sciences, P. O. Box, 50-950 Wroclaw, Poland

Received May 31, 2000; accepted September 11, 2000

DEDICATED TO PROFESSOR J. M. HONIG

The crystal structures of $GdCuAs_2$, $GdCuAs_{1.15}P_{0.85}$, and $GdCuP_{2.20}$ have been investigated by the single crystal and powder methods. While $GdCuAs_2$ (*P*4/*nmm*) retains the tetragonal $HfCuSi_2$ structure (M. Brylak, M. H. Möller, and W. Jeitschko, *J. Solid State Chem.* 115, 305 (1995)), $GdCuAs_{1.15}P_{0.85}$ (*Pmmn*, $a = 3.849(1)$, $b = 3.8501(1)$, $c = 9.871(3)$ Å) and $GdCuP_{2.20}$ (*Pmm*2, $a = 5.3747(9)$, $b = 5.3830(9)$, $c = 9.7376(16)$ Å) undergo orthorhombic distortions. The changes are significant in $GdCuP_{2.20}$: P dimers are formed in the P layer along the *a* direction and there is an additional (but deficient) P site on one side of the layer that links the dimers. The $GdCuAs_{1.15}P_{0.85}$ structure was predicted by the Landau theory. According to this theory the transition from $GdCuAs_2$ to $GdCuAs_{1.15}P_{0.85}$ can be a continous one, the transition from $GdCuAs_{1.15}P_{0.85}$ to $GdCuP_{2.20}$ is a first-order one. The transition to $GdCuP_{2.20}$ occurs with twin formation. The electronic structure and bonding are analyzed by the extended Hückel tight-binding method. The conductivity and magnetic measurements for the arsenide and phosphide are reported. © 2000 Academic Press

1. INTRODUCTION

Intermetallic compounds with 2D square nets of the main group elements are of theoretical and experimental interest to researchers. They show a structural variety in the form of unit cell distortions and help in the understanding of the driving forces of symmetry-breaking in the solid state. Some of them have partially filled bands and an innate tendency to lower their energy by opening a band gap at the Fermi level (1, 2); as a result, a metal-to-semiconductor transition is observed. The electronic instabilities and the resulting distortions are usually referred to as "Peierls," and they are the solid state analogues of molecular Jahn–Teller distortions (3). The presence of the degenerate half-filled states necessitates a large coupling of the vibrational and electronic motions. There is at least one normal mode that will break the degeneracy and lower the energy of the system and, of course, its symmetry. The GdPS (4) and CeAsS (5) structures (members of the *MAB* series) are examples of a 2D Peierls instability, where the layers of P and As atoms distort to form *cis–trans* or zigzag chains, respectively. The electronic structure of the phases was calculated, and the distortion was traced to a band crossing at the Fermi level (6). The deformations are driven by the formation of an energy gap at the Fermi level and result in semiconducting properties. It was suggested that the relative electronegativity of the *M* and *A* atoms dictates whether the distorted or undistorted structure is preferred: a prerequisite for the distortion to occur is a separation of the valence band and metal *d* block (6). The general distortion type square net → zigzag chain can also be found in other phases containing 4^4 nets of the main group atoms, e.g., a distortion from the $ZrSi_2$ to $CaSb_2$ type structures for $YbSb_2$ (7) and $EuSb_2$ (8).

If the Peierls instabilities are important in the 1D and 2D compounds, an *s–p* mixing and next-nearest-neighbor interaction become more important in determining structures with 3D nets. Black phosphorus (orthorombic), As, Sb, and Bi (rhombohedral) have layered structures in which each atom has three short bonds in the layer and relatively long contacts with the atoms in the neighboring layer (9–10). Their structures have traditionally been interpreted as the ones resulting from the Peierls instability inherent in a simple cubic phase with half-filled *p* bands (11–13). Seo and Hoffmann have shown that the calculated Fermi surface for cubic P is not nested, and argued strongly that the structural distortion in black phosphorus has little to do with the Peierls instability (14). They suggested that by forming a nonbonding lone pair band the *s–p* mixing

[1] To whom correspondence should be addressed. 342 Spedding Hall, Ames Laboratory, Iowa State University, Ames, Iowa 50011. Fax: (515) 294-5718. E-mail: franzen@ameslab.gov.

0022-4596/00 $35.00

stabilizes the local distorted geometry in black phosphorus. The *s–p* mixing, as well as the distortion, should decrease down the group due to the *s*-orbital contraction (14), which is observed for P, As, Sb, and Bi. The reverse order of the distortion is predicted from consideration of the Peierls instability. However, in 2*D* compounds the distortions are mainly associated with a Peierls instability, although there is always some *s–p* mixing and the Fermi surface may exhibit no nesting. The concept of the hidden 1*D* Fermi surfaces was developed. According to this approach, nesting associated with hidden surfaces is responsible for the observed symmetry-breaking processes (15, 16).

Among the compounds with 2D nets of main group elements there are the ATB_2 (A = Ca, Sr, Ba; T = Zn, Cd, Mn; B = Sb, Bi (17–21)) phases that are formed of AlB_4-type TB layers and 4^4 nets of Sb or Bi with A atoms intercalated in between. The bands formed mainly by the B p_x and p_y orbitals are quite dispersed and crossed along Γ–X, Γ–Y, and Γ–M symmetry lines in the Brillouin zone (BZ). There is an *s–p* mixing, but the major contribution at the Fermi level comes from the p orbitals. If the number of electrons and electronegativity of a T element are favorable, there will be no overlap of the p_x and p_y bands with other bands and the Fermi level will lie at or near the crossing, an ideal situation for a symmetry lowering and a gap opening. These prerequisites are met in $SrZnSb_2$, where Sb zigzag chains are formed (19).

The $RECuX_2$ (*RE* is a rare earth element, X = P, As, Sb) compounds with the $HfCuSi_2$ structure are also good candidates for a Peierls instability and consequent distortions. Like the ATB_2 phases they have two kinds of X atoms: one half (X_1) form the CuX layer, the other half (X_2) build the square net. Assigning the charges gives the $RE^{+3}Cu^{+1}X_1^{-3}X_2^{-1}$ formula, i.e., six electrons for X_2. The X_2 s and p_z bands can be seen as fully occupied, on the other hand, the X_2p_x and p_y bands are quite disperse, half-occupied, and ready for distortion. But a distortion was not observed. $RECuSb_2$ (22), $RECuAs_2$ (RE = Y, La–Lu except Pm and Eu (23)), $RECu_{1+x}P_{2-x}$ (RE = Gd–Er (24)), $CeCu_{1.09}P_{1.87}$ (a filled $SrZnBi_2$ structure (25)), and $SmCuP_2$ ($SrZnBi_2$ type (26)) were reported to have tetragonal symmetry and an ideal square net of the main group elements. Further single crystal studies on the arsenides showed some additional Cu sites in the structures and in one case a doubling of the c parameter: $LaCu_{1.23(1)}As_2$ adopts a stuffed variant of the $SrZnBi_2$ type, while $CeCu_{1.10(1)}As_2$ and $PrCu_{1.09(1)}As_2$ crystallized with a stuffed version of the $HfCuSi_2$ type (27). The additional Cu atoms enter into the structures on both sides of the still ideal square As net, occupying the apices of the square pyramids. During the investigation of the Ho–Cu–P system, splitting of some peaks for $HoCu_{1+x}P_{2-x}$ was observed; however, the structure was not determined (28). It was an indication of a possible distortion of the tetragonal cell and this structural change could be triggered by a symmetry-breaking process in the P net. We looked more closely into $RECuAs_2$ and $RECuP_2$ and observed a peak splitting also for Gd, Er phosphides. The corresponding Gd, Ho, and Er arsenides were found to have tetragonal $HfCuSi_2$ structures.

We focused our research on $GdCuP_2$ and saw interesting structural changes on going from the arsenide to the phosphide. The Guinier powder pattern of the phosphide could be originally indexed in space group $P2/n$ with $a = 3.7892(6)$, $b = 9.751(1)$, $c = 3.7904(5)$ Å and $\beta = 90.631(9)^\circ$ (29). According to the Landau theory, a continuous symmetry-breaking transition from a tetragonal cell of $GdCuAs_2$ (23) to a monoclinic cell of $GdCuP_2$, maintaining the same principal axis direction, is stepwise through orthorhombic symmetry. The orthorhombic cell with space group *Pmmm* has been experimentally found for a mixed $GdCuAs_{1.15}P_{0.85}$ arsenophosphide. However, the pure phosphide turned out to have an additional but deficient P site and a larger orthorhombic cell (30). Twinning of the phosphide crystals, which results from the symmetry-breaking process, was observed during the X-ray work. Here we report the structures and magnetic and electrical properties of $GdCuX_2$ (X is P, As or both) and analyze the observed distortions.

2. EXPERIMENTAL

2.1. Synthesis

The starting materials were powdered gadolinium (99.9%, Alfa Aesar), copper (99.5%, Alfa Aesar), amorphous red phosphorus (99%, Alfa Aesar), and arsenic (99.99%, Alfa Aesar). Weighing and handling of the samples were performed in an Ar-filled glove box. The powders with total mass 0.5–1.0 g were intimately mixed, pressed to a pellet under a pressure of 2000 kg using a 10-mm dial tool, and sealed in evacuated silica tubes. For the X-ray powder analysis the samples with compositions $GdCuAs_xP_{2-x}$ (x = 0, 0.33, 0.67, 1.00, 1.33, 1.67, 2.00) were heated at the rate of 20°C/h at 600°C, kept at this temperature for 48 h, and furnace-cooled. The samples were ground, pressed, sealed, heated at 40°C/h to 800°C, kept at 800°C for 3 days, and cooled. The second step was repeated once more with the heat treatment period increased to 7 days. After each step the Guinier powder patterns were taken to check for sample homogeneity.

Single crystals of $GdCuAs_2$, $GdCuAs_{1.15}P_{0.85}$, and $GdCuP_{2.20}$ were obtained by the iodine gas transport technique in a zone furnace: length of the silica tubes was ~ 200 mm, inner diameter 10 mm, the pellets were placed at the hot end at 900°C, the temperature of the cold end was 800°C. The initial compositions and iodine concentrations were $GdCuAs_2$ and 0.8 mg/cm^3, GdCuAsP and 0.45 mg/cm^3, $GdCuP_2$ and 1.0 mg/cm^3. The samples were heated to 20°C/h, kept for 2 weeks, and then furnace-cooled.

Air-stable single crystals were obtained as shiny square plates at the cold end of the tubes.

For the energy dispersive spectroscopic (EDS) analysis single crystals of CuP_2 were prepared by the above described gas transport method.

2.2. X-Ray Analysis

The powder patterns of the samples were recorded using Guinier cameras (Enraf Nonius, Cu$K_{\alpha 1}$) with Si as an internal standard and the exposed and developed films were laser scanned to obtained peak positions. The lattice parameters (Table 1) were derived by the least-squares method using the CSD program package (31). Peak splitting was observed for the arsenophosphides and the phosphide, but different peaks were split in two cases. The phosphide has the most intense and some smaller peaks well split, which is seen even on the diffractogram (Fig. 1); on the other hand, the mixed compounds have other peaks split and this splitting can be seen only on Guinier patterns. The powder patterns (Fig. 1) were also taken at the Siemens D5000 ($GdCuAs_2$, Cu$K_{\alpha 1}$) and Scintag (GdCuPAs and $GdCuP_2$, solid state cooled detector, Cu$K_{\alpha 1}$ and Cu$K_{\alpha 2}$) diffractometers. The pattern of $GdCuAs_2$ was well indexed in the P4/*nmm* space group, and that of the phosphide was indexed, initially, in the *P*2/*n* space group with $a = 3.7892(6)$, $b = 9.751(1)$, $c = 3.7904(5)$ Å, and $\beta = 90.631(9)^\circ$. From the Landau theory a mixed arsenophosphide with the *Pmmn* space group was predicted, and the observed reflections of the synthesized $GdCuAs_{2-x}P_x$ phases were found to correspond to this group (29).

Single-crystal methods were used to confirm the indexing results and to refine the atomic parameters. Crystals in the form of the square plates, obtained by the gas transport technique from the $GdCuAs_2$, GdCuAsP, and $GdCuP_2$ samples, were checked by the Laue method. Crystals of the arsenide and arsenophosphide were not twinned; their data sets were collected and their structures were easily refined (Tables 2–4) using the SHELXTL program (32). Only the peaks relevant to the *Pmmn* space group and presented

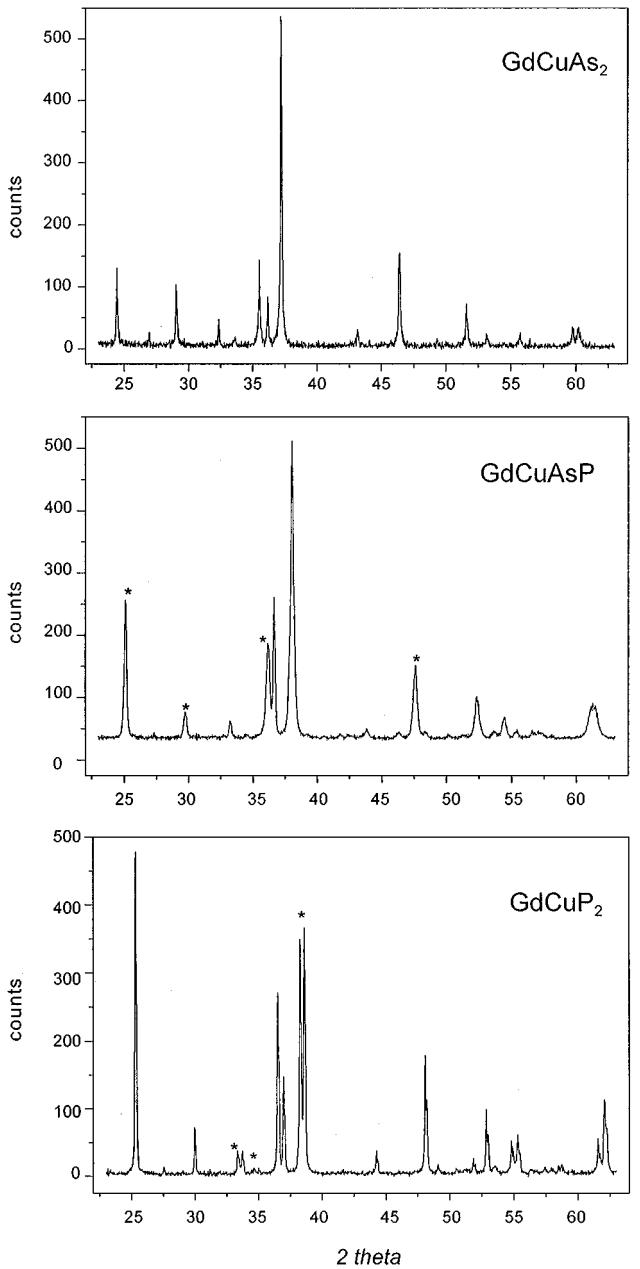

FIG. 1. Powder patterns of $GdCuAs_2$, GdCuAsP, and $GdCuP_2$ (all are the sample initial compositions). Asterisks indicate splitting of the low angle peaks.

TABLE 1
Powder Lattice Parameters for $GdCuX_2$

Composition	Space group	*a*, Å	*b*, Å	*c*, Å	*b*/*a*	*V*, Å^3
$GdCuAs_2$	*P*4/*nmm*	3.9112(9)	3.9112(9)	9.930(3)	1.0000	152.9
$GdCuAs_{1.67}P_{0.33}$	*Pmmn*	3.883(2)	3.890(2)	9.908(4)	1.0018	149.7
$GdCuAs_{1.33}P_{0.67}$	*Pmmn*	3.850(2)	3.867(2)	9.888(4)	1.0044	147.2
GdCuAsP	*Pmmn*	3.8314(8)	3.8443(8)	9.8613(9)	1.0034	145.2
$GdCuAs_{0.67}P_{1.33}$	*Pmmn*	3.8072(9)	3.8278(9)	9.843(2)	1.0054	143.4
$GdCuAs_{0.33}P_{1.67}$	*Pmmn*	3.793(1)	3.812(1)	9.822(2)	1.0050	142.0
$GdCuP_{2.16}$[a]	*Pmm*2[b]	5.3284(1)	5.3868(1)	9.7487(3)	1.0110	139.9

[a] Composition from the Rietveld refinement.
[b] Not a superstructure of $GdCuAs_{0.33}P_{1.67}$.

lattice parameters were observed on the two-dimensional CCD detector for the arsenophosphide. Statistical mixtures of P and As was found on both sites and the composition was refined to $GdCuAs_{1.15}P_{0.85}$.

Although all examined single crystals of the phosphide looked ideal under the microscope, they were twins under X-rays. Analysis of the Laue pictures indicated that the plane of twinning was 010 (*b* is the largest axis, original monoclinic setting). Rotation around *b* gave 9.76 Å, rotation along the diagonal in the *ac* plane gave 5.35 Å, but

TABLE 2
Crystal Data and Structure Refinements

Empirical formula	$GdCuAs_2$	$GdCuAs_{1.15}P_{0.85}$	$GdCuP_{2.20}$
Space group	*P*4/*nmm* (No. 129)	*Pmmn* (No. 59)	*Pmm*2 (No. 25)
Unit cell dimensions, Å	$a = 3.917(1)$	$a = 3.8468(10)$	$a = 5.3747(9)$
	$c = 9.939(1)$	$b = 3.8497(11)$	$b = 5.3830(9)$
		$c = 9.871(3)$	$c = 9.7375(16)$
Z	2	2	4
Density (calculated)	8.072 g/cm^3	7.572 g/cm^3	6.825 g/cm^3
Diffractometer	Siemens P4	Siemens SMART	Siemens SMART
2θ range	4.10 to 53.50°	4.12 to 57.84°	4.18 to 56.88°
Index ranges	$-1 \le h \le 5$,	$-5 \le h \le 4$,	$-7 \le h \le 7$,
	$-5 \le k \le 5$, $-12 \le l \le 12$	$-4 \le k \le 5$, $-12 \le l \le 10$	$-6 \le k \le 7$, $-12 \le l \le 12$
Reflections collected	900 [$R\sigma = 0.0319$]	919 [$R\sigma = 0.0362$]	2506 [$R\sigma = 0.0328$]
Abs. Correction/Program	empirical from ψ-scan	empirical/SADABS	empirical/SADABS
Independent reflections	127 [$R_{int} = 0.0696$]	228 [$R_{int} = 0.0526$]	794 [$R_{int} = 0.0444$]
Reflections with $I > 2\sigma(I)$	125	208	723
Completeness to max 2θ	100.0%	89.8%	95.4%
Data/restraints/par.	127/0/12	228/0/20	794/1/47
Goodness-of-fit on F^2	1.334	1.027	1.165
Final R indices ($I > 2\sigma(I)$]	$R_1 = 0.0257$,	$R_1 = 0.0201$,	$R_1 = 0.0359$,
	$wR_2 = 0.0590$	$wR_2 = 0.0453$	$wR_2 = 0.0983$
R indices (all data)	$R_1 = 0.0265$	$R_1 = 0.0241$,	$R_1 = 0.0395$,
	$wR_2 = 0.0593$	$wR_2 = 0.0465$	$wR_2 = 0.1003$
Extinction coefficient	0.038(3)	0.0087(14)	0.0096(6)
Largest diff. peak/hole	1.468/−2.289 e/Å^3	0.875/−1.103 e/Å^3	2.921/−2.514 e/Å^3

$R_{int} = \sum|F_o^2 - F_o^2 \text{ mean}|/\sum F_o^2$.
$R\sigma = \sum\sigma F_o^2/\Sigma F_o^2$.
$R_1 = \sum||F_o| - |F_c||/\sum|F_o|$.
$R_w = (\sum w \times (F_o^2 - F_c^2)^2/\sum w \times (F_o^2)^2)^{1/2}$, $w = 1/(\sigma^2(F_o^2) + (a \times P)^2 + b \times P)$.
GoF $= (\sum w \times (F_o^2 - F_c^2)^2/(n-p))^{1/2}$ with $w = 1/(\sigma^2(F_o^2) + (a \times P)^2 + b \times P)$, n is the number of observed reflections, p is number of parameters refined.

Note. $T = 293(2)$ K, Mo$K\alpha$ radiation, graphite monochromator, the refinement method was full-matrix least-squares on F^2.

rotation along a showed weak superstructure reflections, doubling the current monoclinic a parameter. Further investigation was done on a Siemens SMART diffractometer with a CCD detector. Indexing of the reflections resulted in an orthorhombic unit cell with $a = 5.3747(9)$, $b = 5.3830(9)$, and $c = 9.7375(16)$ Å. In this case the relationship between the monoclinic and larger orthorhombic cells for the phosphide is obvious: $\boldsymbol{b}_{mon} = \boldsymbol{c}_{ort}$, $\boldsymbol{a}_{mon} = \frac{1}{2}(\boldsymbol{a}_{ort} + \boldsymbol{b}_{ort})$, $\boldsymbol{c}_{mon} = \frac{1}{2}(\boldsymbol{a}_{ort} - \boldsymbol{b}_{ort})$ and $\beta_{mon} = \angle(\boldsymbol{a}\boldsymbol{b}_{ort})$.

The structure of the phosphide was solved in space group *Pmm*2 (Table 2). During the refinement (SHELXTL program (32)) a significant residual electron density was observed on one side of the P net. On the basis of the interatomic distances the site was assigned to additional P atoms in the structure (P6 in Tables 5, 6) and this resulted in the $GdCuP_{2.20}$ composition, which was later confirmed by an EDS analysis. The refinement was successful with the twinning rule:

$$\begin{pmatrix} 0 & 1 & 0 \\ 1 & 0 & 0 \\ 0 & 0 & -1 \end{pmatrix} \begin{pmatrix} \boldsymbol{a} \\ \boldsymbol{b} \\ \boldsymbol{c} \end{pmatrix} = \begin{pmatrix} \boldsymbol{a}' \\ \boldsymbol{b}' \\ \boldsymbol{c}' \end{pmatrix}.$$

The relative arrangement of the atoms, except for P6, in the $GdCuP_{2.20}$ structure was similar to those in $GdCuAs_2$ and $GdCuAs_{1.15}P_{0.85}$. In the process of the refinement of the P1–P4 sites, which are located in the CuP layer and result from one atomic site in the parent $HfCuSi_2$ structure, very close isotropic displacement factors (U_{eq}) and

TABLE 3
Atomic and Equivalent Isotropic Displacement Parameters (U_{eq}, Å^2) for $GdCuAs_2$ (Space Group *P4/nmm*, $HfCuSi_2$ Type) and $GdCuAs_{1.15}P_{0.85}$ (Space Group *Pmm*2)

		$GdCuAs_2$					$GdCuAs_{1.15}P_{0.85}$			
Atom		x	y	z	U_{eq}		x	y	z	U_{eq}
Gd	2*c*	$\frac{1}{4}$	$\frac{1}{4}$	0.23844(8)	0.0083(4)	2*a*	$\frac{1}{4}$	$\frac{1}{4}$	0.24108(4)	0.0159(3)
Cu	2*b*	$\frac{3}{4}$	$\frac{1}{4}$	$\frac{1}{2}$	0.0117(6)	2*b*	$\frac{1}{4}$	$\frac{3}{4}$	0.49989(12)	0.0192(3)
*X*1[a]	2*c*	$\frac{1}{4}$	$\frac{1}{4}$	0.65810(18)	0.0091(6)	2*a*	$\frac{1}{4}$	$\frac{1}{4}$	0.65545(16)	0.0172(6)
*X*2[b]	2*a*	$\frac{3}{4}$	$\frac{1}{4}$	0	0.0142(6)	2*b*	$\frac{1}{4}$	$\frac{3}{4}$	0.00005(11)	0.0256(5)

[a] *X*1 = 32.8(8)%As + 67.2(8)%P for $GdCuAs_{1.15}P_{0.85}$.
[b] *X*2 = 82.1(6)%As + 17.9(6)% for $GdCuAs_{1.15}P_{0.85}$.

TABLE 4
Interatomic Distances (Å) in $GdCuAs_2$ and $GdCuAs_{1.15}P_{0.85}$

Atoms	$GdCuAs_2$	$GdCuAs_{1.15}P_{0.85}$	Atoms	$GdCuAs_2$	$GdCuAs_{1.15}P_{0.85}$
Gd–4*X*1	2.9545(9)	2.9065(7)	4*X*1–4Cu	2.5109(12)	2Cu at 2.4598(13)
4*X*2	3.0745(7)	3.0601(11)			2Cu at 2.4622(13)
4Cu	3.2548(8)	2Cu at 3.1986(12)	4Gd	2.9545(9)	2.9065(7)
		2Cu at 3.1995(12)			
			*X*2–4*X*2	2.7697(7)	2.7211(5)
Cu–4*X*1	2.5109(12)	2*X*1 at 2.4598(13)	4Gd	3.0745(7)	3.0601(11)
		2*X*1 at 2.4622(13)			
4Cu	2.7697(7)	2.7211(5)			

Note. *X* is As for $GdCuAs_2$ and As/P for $GdCuAs_{1.15}P_{0.85}$.

correlated *z* parameters were obtained. In the final steps all their U_{eq}'s were kept the same, and the *z* coordinates of P4 and P5 were related to *z*'s of P1 and P2 by $(1 - z_{P1,P2})$ with *z*'s of P1 and P2 being equal. The refinement with these constraints was more stable and converged to $R = 0.0359$. This indicated that the CuP block of the structure is very rigid and undergoes very small distortions in $GdCuP_{2.20}$.

On the other hand, the P5 atoms showed significant shifts in the *a* direction from the ideal square lattice sites, but changes along *b* and *c* were small (Table 4). The twinning in the *ab* plane with *a* and *b* axes superimposed (this is discussed later) plus the large shifts along *a* obscured the electron density map in the P5 net and did not allow satisfactory refinement of the *y* and *z* parameters of P5. Nevertheless the distortion of the P5 net and the formation of the phosphorus dimers was obvious in $GdCuP_{2.20}$.

The structure of the phosphide was also refined by the full-profile Rietveld technique (Fig. 2), using the CSD package (31). The atomic parameters were close to those from the single-crystal data; the composition changed slightly to $GdCuP_{2.16}$. The formula $GdCuP_{2.20}$, based on the refinement of the single-crystal data, is used further since the band structure calculations and structure analysis are based on the single crystal results.

TABLE 5
Atomic and Equivalent Isotropic Displacement Parameter (U_{eq}, Å^2) for $GdCuP_{2.20}$ (Space Group *Pmm*2)

Atom		*x*	*y*	*z*	U_{eq}
Gd1	1*b*	0	1/2	0.2361(2)	0.011(1)
Gd2	1*c*	1/2	0	0.2459(2)	0.008(1)
Gd3	1*d*	1/2	1/2	0.7587(1)	0.007(1)
Gd4	1*a*	0	0	0.7756(2)	0.010(1)
Cu	4*i*	0.2480(2)	0.2506(5)	0.5026(5)	0.010(1)
P1	1*b*	0	1/2	0.6546(3)	0.008(1)
P2	1*c*	1/2	0	0.6546(3)	0.008(1)
P3	1*d*	1/2	1/2	0.3454(3)	0.008(1)
P4	1*a*	0	0	0.3454(3)	0.008(1)
P5	4*i*	0.2890(6)	0.2453(16)	0.0049(12)	0.018(1)
P6[a]	1*a*	0	0	0.1074(11)	0.024(3)

[a] Occupancy is 78(3)%.

2.3. EDS Analysis

EDS quantitative elemental analysis of phosphide crystals was performed on a JEOL 840A scanning electron microscope, equipped with an IXRF Systems Iridium X-ray analyzer. The single crystals of CuP_2, prepared by the gas transport technique, were used as standards to determine the Cu/P ratio in the gadolinium copper phosphide. The

TABLE 6
Selected Interatomic Distances (Å) in $GdCuP_{2.20}$

Atoms	Distances	Atoms	Distances
Gd1–2P3	2.8904(12)	Cu–P2	2.403(4)
2P4	2.8943(12)	P1	2.418(4)
2P6	2.969(5)	P4	2.437(4)
4P5	3.059(9)	P3	2.446(4)
4Cu	3.211(4)	Cu	2.666(2)
		Cu	2.686(6)
Gd2–2P4	2.8564(11)	Cu	2.697(6)
2P3	2.8603(11)	Cu	2.709(2)
4P5	2.922(10)		
2P6	3.007(5)	P5–P5	2.268(7)
4Cu	3.146(4)	P6	2.270(9)
		P5	2.641(17)
Gd3–2P2	2.8721(11)	P5	2.742(17)
2P1	2.8760(11)	P5	3.106(7)
4P5	2.985(10)		
4Cu	3.140(4)	P6–4P5	2.270(9)
Gd4–2P1	2.9342(12)		
2P2	2.9380(12)		
4P5	3.023(10)		
2P6	3.231(10)		
4Cu	3.266(4)		

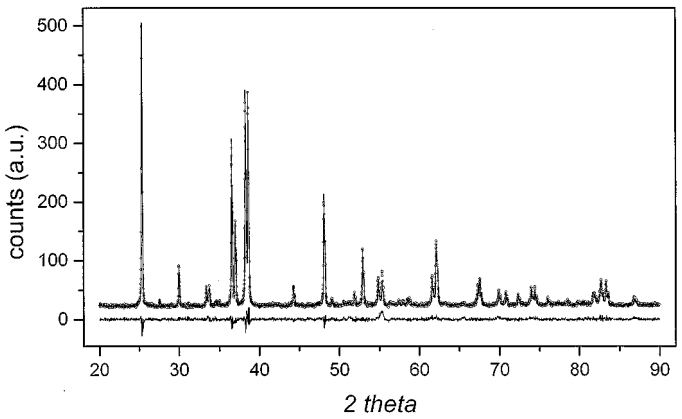

FIG. 2. Observed (circles) and calculated (solid line) profiles and difference between them for the gadolinium copper phosphide.

lattice parameters of CuP_2 crystals were checked on a single crystal diffractometer. A data set for one crystal was collected and the structure was refined to check the composition. No oxygen was observed in the crystals of CuP_2 and the gadolinium copper phosphides. The analysis of the three crystals (one is shown in Fig. 6) gave P/Cu ratios of 2.32, 2.08, and 2.11, which proved an additional P (not Cu or O) site in the structure. The mean (2.17) of these measurements was close to the results of the single-crystal refinement ($GdCuP_{2.20}$).

2.4. Electric and Magnetic Measurements

Conductivities were measured on powders of the arsenide and a single crystal of the phosphide with a computer automated setup, using a standard DC two-probe method. Electrode connections were made with 50-μm silver wires and indium solder. Samples were cooled in a He flow cryostat. The temperature was measured with a LakeShore DT 470 silicon diode temperature sensor located close to the crystal. Resistivities were measured between 285 and 4 K in increments of 2 K. No indication of thermal hysteresis was observed, showing good temperature equilibrium throughout the measurement cycle.

Magnetic measurements were performed on powder of the arsenide and on powder and a single crystal of the phosphide in the temperature range 1.7–300 K and in applied magnetic fields up to 50 kOe employing a Quantum Design MPMS-5 SQUID magnetometer. Antiferromagnetic ordering at low temperatures is observed for both compounds.

2.5. Band Structure Calculations

Band structure calculations were performed by the extended Hückel tight binding (EHTB) method (33). Lattice and atomic parameters from the single crystal refinements of $GdCuAs_2$, $GdCuAs_{1.15}P_{0.85}$, and $GdCuP_{2.20}$ were used in the calculations. For the COOP analysis the X^{1-} and $Cu_2X_2^{2-}$ layers in $GdCuAs_{1.15}P_{0.85}$ were assumed to be occupied only by As and P, respectively. The additional P6 site in the $GdCuP_{2.20}$ was considered fully occupied (the resulting composition was $GdCuP_{2.25}$), but later the electron number was taken as that for the real composition in order to have the right position of the Fermi level. The orbital energies and coefficients for the Slater-type orbitals were taken from (34). The parameters for Gd and Cu were refined by the alternating charge iteration technique, while the As and P parameters were kept constant (Table 7).

TABLE 7
Parameters for the Extended Hückel Tight-Binding Calculations

Atom	Orbital	H_{ii}, eV $GdCuAs_2$	H_{ii}, eV, $GdCuAs_{1.15}P_{0.85}$[a]	H_{ii}, eV, $GdCuP_{2.20}$[b]	ξ_1	c_1^c	ξ_2	c_2^c
Gd	6*s*	− 7.61	− 7.62	− 7.14	1.369	1.00		
Gd	6*p*	− 5.03	− 5.04	− 4.62	1.369	1.00		
Gd	5*d*	− 8.05	− 8.07	− 7.45	2.747	0.7184	1.267	0.4447
Cu	4*s*	− 9.46	− 9.16	− 8.46	2.20	1.00		
Cu	4*p*	− 5.30	− 5.07	− 4.53	2.20	1.00		
Cu	3*d*	− 14.55	− 14.10	− 12.97	5.95	0.5933	2.30	0.5744
As	4*s*	− 16.22	− 16.22		2.23	1.00		
As	4*p*	− 12.16	− 12.16		1.89	1.00		
P	3*p*		− 18.60	− 18.60	1.75	1.00		
P	3*p*		− 14.00	− 14.00	1.30	1.00		

[a] The composition GdCuAsP with As on the *X*1 site and P on the *X*2 site was taken for calculations.
[b] The P6 site was assumed to be fully occupied, that gave $GdCuP_{2.25}$ for the calculations.
[c] Coefficients used in the double-zeta Slater-type orbitals.

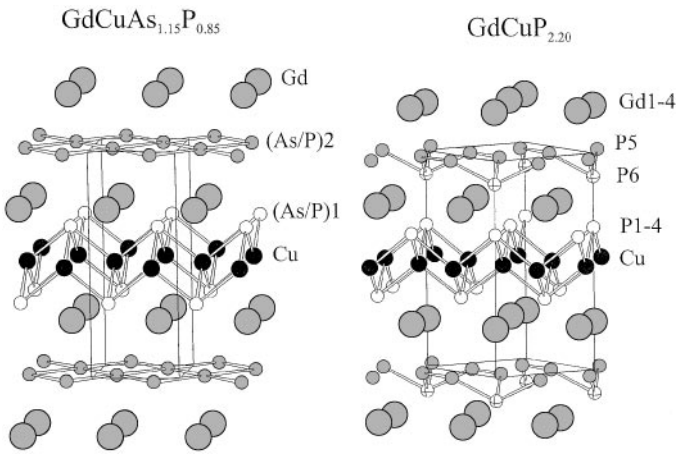

FIG. 3. Structures of $GdCuAs_{1.15}P_{0.85}$ and $GdCuP_{2.20}$.

3. RESULTS AND DISCUSSION

3.1. Structures Description

We observed no distortions of the tetragonal $GdCuAs_2$ structure ($P4/nmm$ space group, $HfCuSi_2$ type), and its powder lattice parameters (Table 1) agreed well with the reported ones: $a = 3.9105(4)$ and $c = 9.929(2)$ Å (23). The mixed arsenophosphides adopt a previously unknown orthorhombic distorted version of the $HfCuSi_2$ structure with space group $Pmmn$ (Fig. 3). In the refined structure of $GdCuAs_{1.15}P_{0.85}$ both sites are statistically occupied and this can be assumed for the rest of the arsenophosphides. The unit cell volume decreases monotonically with the P content but the distortion has an opposite trend (Fig. 4).

$GdCuP_{2.20}$ has an orthorhombic cell with twice the cell volume of $GdCuAs_{1.15}P_{0.85}$ (Fig. 3). As mentioned before, the CuP layer is rigid and therefore undergoes only small distortions. Each Cu atom has four P atoms at 2.403–2.446 Å (Table 4), and the bond variations can be attributed to the symmetry lowering. This kind of building block, composed of a transition metal tetrahedrally coordinated by a main group element, can be found in many parent structures, e.g., $BaAl_4$, $ThCr_2Si_2$, $CaBe_2Ge_2$, and $HfCuSi_2$, with a large number of representatives among ternary phases.

The P layer undergoes a severe distortion in the a direction, resulting in P5–P5 dimer formation with short bonds of 2.268(7) Å and large distances of 3.106(7) Å between the dimers (Fig. 5). Shifts along the b axis are small and do not lead to a strong bond formation in that direction. Dimers are linked with each other along a by the additional phosphorus atoms (P6) on one site of the P5 layer. This additional phosphorus site stabilizes dimers by not allowing a bond formation along the b axis. Energetics of the distortion and bond formation is discussed below. The P–P distance of 2.268 Å in the dimers is close to the single bond distances of 2.22–2.25 Å in the layers of the black phosphorus (9a). The P5–P6 distances (δ) of 2.270 Å (Fig. 5) are a little larger but also close to those in the black phosphorus.

The P5–P5 and P5–P6 bonds are similar to the ones found in the rare-earth phosphides with relatively high amounts of phosphorus. In CeP_2 (35) and LaP_2 (36) phosphorus atoms are joined into fragments of the zigzag chains of 4 or 3 and 5 atoms with $\delta_{P-P} = 2.404$–2.453 Å and $\delta_{P-P} = 2.197$–2.314 Å, respectively. In LaP_5 (37) and LaP_7 (38) phosphorus forms a layer and a 3D framework with $\delta_{P-P} = 2.167$–2.216 Å and $\delta_{P-P} = 2.1072$–2.246 Å. However, the structural pattern of P atoms, as found in the structure of $GdCuP_{2.20}$, was not observed in any binary or other ternary phases.

3.2. Symmetry-Breaking Transitions and Landau Theory

When questions arise about the nature of phase transitions and correctness of a structure, researchers resort to the Landau theory (39–41) for answers. The theory can

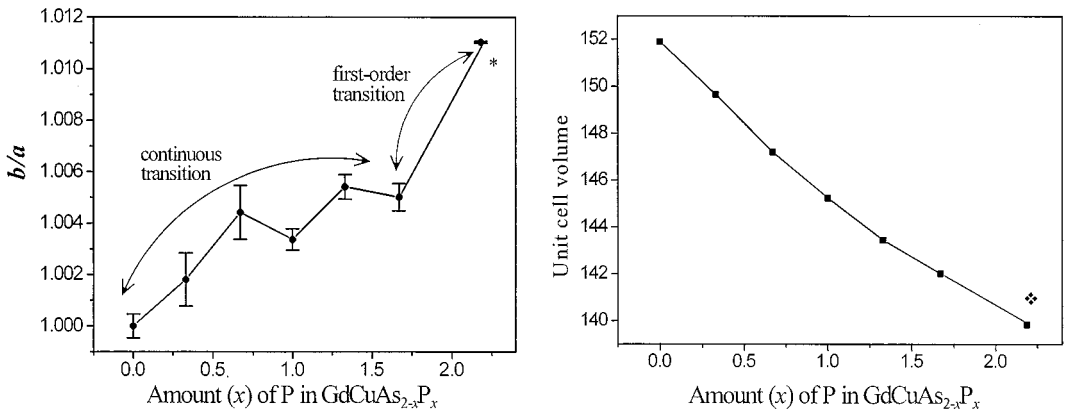

FIG. 4. b/a ratio (left) and unit cell volume (right) versus phosphorus amounts. * Composition of the phosphide is $GdCuP_{2.16}$ (Rietveld refinement) $*\frac{1}{2}V_{unit\ cell}$ of $GdCuP_{2.16}$.

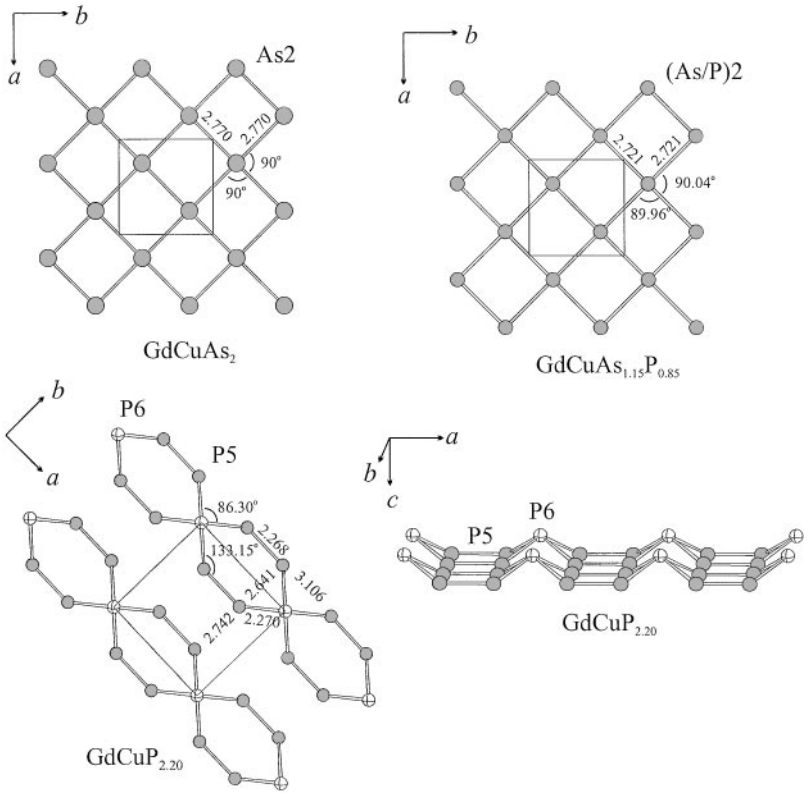

FIG. 5. As, As/P, and P layers in $GdCuAs_2$, $GdCuAs_{1.15}P_{0.85}$, and $GdCuP_{2.20}$.

provide a structural model for one of the phases during a continuous symmetry-breaking process as it did for the low-temperature modification of $CaAl_4$ (42). But its main benefit is that it provides symmetry constraints in cases of symmetry-breaking transitions.

Application of the Landau theory helped us to predict a new structure despite the fact that the initial structure of the phosphide was incorrect. From the powder data the structure of the phosphide was believed to be monoclinic with space group $P2/n$. Similarities in the powder patterns of the phosphide and arsenide indicated that the symmetry-breaking transition from the arsenide to the phosphide might be continuous (29). From the Landau theory such a continuous transition from a tetragonal cell of the arsenide to a monoclinic cell of the phosphide, maintaining the same principle axis direction must be stepwise through orthorhombic symmetry. Accordingly the orthorhombic cell with space group *Pmmm* was considered and it was experimentally confirmed for arsenophosphides ($GdCuAs_{1\cdot15}P_{0.85}$ structure). However, the phosphide turned out to have a larger orthorhombic unit cell and an additional P site.

3.2.1 Transition from $GdCuAs_2$ to $GdCuAs_{1.15}P_{0.85}$. The first consideration in the Landau theory is the determination of a wave vector $\boldsymbol{k}$ (or set of equivalent wave vectors in a star), corresponding to the distortion in the sense that any lost translation (vectors $\boldsymbol{T}_i$) yield nonintegral values for $\boldsymbol{k}\cdot\boldsymbol{T}_i/2\pi$. Since there is no superstructure created by the distortion from tetragonal $GdCuAs_2$ to orthorhombic $GdCuAs_{1.15}P_{0.85}$, the $\boldsymbol{k}$ vector of the distortion is $\boldsymbol{k}=0$. The second step is to find an irreducible representation corresponding to the $\boldsymbol{k}$ vector of the interest. Since the wave vector under consideration is $\boldsymbol{k}=0$, the irreducible representations are isomorphous with those of the point group D_{4h} for $GdCuAs_2$.

There are eight one- and two two-dimensional such representations. The two-dimensional representations would result in four symmetry elements, corresponding to a monoclinic subgroup, and are not of interest. All, except the totally symmetric, one-dimensional representations result in a loss of all symmetry operations with character -1, and they lead according to Landau theory to a halving of the number of the rotational symmetry elements and thus to space groups with eight essential symmetry elements. Four of the seven subgroups have orthorhombic unit cells but only two (from the B_{1g} and B_{2g} representations) preserved the horizontal plane and inversion center. The space group *Pmmn*, corresponding to B_{1g} (Table 8), is the one found experimentally in $GdCuAs_{1.15}P_{0.85}$.

The third consideration of Landau theory is to determine whether any third-order symmetry combination of basis

TABLE 8
One-Dimensional Irreducible Representation B_{1g} of *P4/nmm* at Γ

g	$\in$	C_{4z}	C_{4z}^3	C_{2z}	C_{2x}	C_{2y}	$C_{2(x+y)}$	$C_{2(x-y)}$
$\chi(g)$	1	−1	−1	1	1	1	−1	−1
g	i	$\bar{C}_{4z}$	$\bar{C}_{4z}^3$	σ_z	σ_x	σ_y	σ_{x+y}	σ_{x-y}
$\chi(g)$	1	−1	−1	1	1	1	−1	−1

vectors is invariant under all symmetry operations of the group. If such a third-order invariant exists, then a third-order term appears in the Gibbs free energy expansion in the order parameter η, and the transition must be discontinuous (40, 41). In the case of a one-dimensional irreducible representation the particle density, ρ, can be expressed in terms of that of symmetrical form, ρ^0, and one basic function, ϕ:

$$\rho = \rho^0 + \eta\phi.$$

This function is symmetric to one half and antisymmetric to the other half of symmetry elements in B_{1g} (see Table 8); e.g., C_2^z takes ϕ into itself, but C_4^z transforms ϕ into $-\phi$. Thus no third-order invariant combination can be formed from a basis function of this irreducible representation. It follows that $P4/nmm \rightarrow Pmmn$ with $\boldsymbol{a}_{\text{ort}} = \boldsymbol{a}_{\text{tet}}$, $\boldsymbol{b}_{\text{ort}} = \boldsymbol{b}_{\text{tet}}$, and $\boldsymbol{c}_{\text{ort}} = \boldsymbol{c}_{\text{tet}}$ meets the Landau conditions for a second-order phase transition.

Finally, in order for a second-order transition from $GdCuAs_2$ to $GdCuAs_{1.15}P_{0.85}$ to be allowed the Lifshitz criterion must be met. This criterion is used to determine whether a minimum in the Gibbs free energy as a function of wave vectors is fixed by symmetry at the reciprocal space point to which the transition corresponds. In the case under consideration inversion is in the point group of the wave vector and thus this point meets the Lifshitz condition.

3.2.2. Transition from $GdCuAs_{1.15}P_{0.85}$ to $GdCuP_{2.20}$. The transition from $GdCuAs_{1.15}P_{0.85}$ (space group *Pmmn*) to $GdCuP_{2.20}$ (space group *Pmm2*) is between two different subgroups of the parent *P4/nmm* symmetry of the $GdCuAs_2$ structure. The *a* and *b* directions in the arsenophosphide and phosphide correspond to *a* and *b* of *P4/nmm* for $GdCuAs_{1.15}P_{0.85}$ and to the face diagonals of *P4/nmm* for $GdCuP_{2.20}$, respectively. Thus, the phases are not in a group–subgroup relationship; therefore, this is a first-order transition.

3.2.3. Twinning of phosphide crystals. During the X-ray studies all tested crystals of the phosphide were twins although they looked ideal under the microscope (Fig. 6). The twinning plane was 001 with the *a* and *b* axes of the twin parts being superimposed. Since the largest shifts are in the P layer of $GdCuP_{2.20}$, divergence of the distortion directions results in twin formation. In the (As/P)2 layer of $GdCuAs_{1.15}P_{0.85}$ each atom has four neighbors at 2.721 Å (Fig. 5); in the P5 layer of $GdCuP_{2.20}$ dimers with P–P distance 2.269 Å are formed (Fig. 5). There are two ways of going from the (As/P)2-type layer to the real P5 layer of $GdCuP_{2.20}$: one is to form dimers along *a*, the other is along *b*. At the initial stage of crystal growth, when the lattice is not well defined, these two ways will not differ in energy with respect to the already formed lattice and are equally probable at the temperature of the experiment. So one twin will have dimers along *a*, the other will have them along *b* (the *b* axis for the second twin will be its *a* axis). That is what is experimentally found for $GdCuP_{2.20}$ (Fig. 6).

3.3. *Electronic Structure and Bonding in $GdCuP_{2.20}$*

As mentioned in the Introduction, symmetry-breaking transitions involving 2*D* nets are the result of the instabilities that lead to energy lowering. Without the P6 site, the structure of $GdCuP_{2.20}$ would fit ideally into the classical 2*D* Peierls distortion case and probably would undergo a change similar to that in $SrZnSb_2$ (19). However, the situation is different: instead of *cis–trans* or zigzag chains the P5–P5 dimers are formed and the dimers are joined by the P6 atoms in the *a* direction to produce double chains (Fig. 5). To understand this unusual geometry we will break the distortion process into two steps. At the beginning we will analyze the instability of the P5 square net, and then we will try to explain the role of P6 atoms.

We start with an electron count in the hypothetical tetragonal structure of $GdCuP_2$ ($x = y = 0.25$ for P5) with no additional P6 sites. The Gd1–Gd4 atoms have no short metal–metal bonds (Table 4) and therefore may be counted as Gd^{3+} in agreement with the results of the magnetic susceptibility measurements. The P1–P4 atoms have no close anion neighbors and can safely be assumed to be P^{3-}. The shortest Cu–Gd and Cu–Cu distances are 3.140–3.266

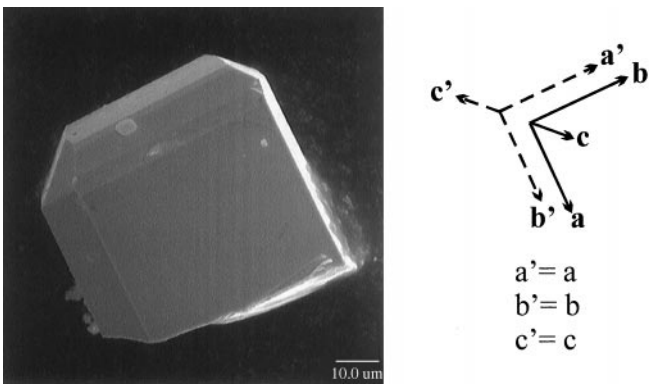

FIG. 6. A twin crystal of the phosphide and the twinning rule.

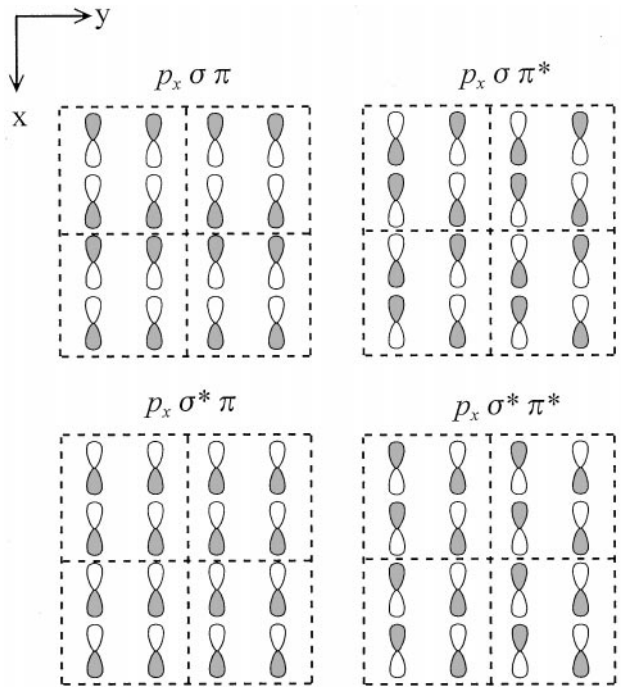

FIG. 7. Molecular orbitals (MOs) from the p_x orbitals of the P5 atoms.

and 2.666–2.709 Å in the real structure; this is typical of Cu^+ (d^{10}) as it is mostly found in pnictide and chalocogenide systems. Based on the above oxidation state assignments the electronic structure can be described as $(Gd(1–4)^{3+})(Cu^+)(P(1–4)^{3-})(P(5)^-)$.

Since the energies of P s orbitals are low and the p_z orbitals do not overlap much in the xy plane, the s and p_z bands of P5 will lie below the Fermi level and will be fully occupied. So far, we neglect an s–p mixing. There are four P5 atoms in the unit cell and therefore four types of molecular orbitals ($\sigma\pi$ and $\sigma\pi^*$ bonding, $\sigma^*\pi$ and $\sigma^*\pi^*$ antibonding) can be formed from the remaining half-filled p_x and p_y atomic orbitals (Fig. 7). Each MO generates a band and the evolution of the bands along Γ–X is presented in Fig. 8a. The $p_x\sigma\pi^*$ and $p_x\sigma^*\pi$ bands cross and the same will be observed for $p_y\sigma\pi^*$ and $p_y\sigma^*\pi$ bands along Γ–Y. The Fermi level resides at the crossing, the ideal situation for a Peierls instability and a distortion.

Distortion from the tetragonal unit cell to the observed orthorhombic one, while retaining $x = y = 0.25$ for P5, will break only the degeneracy of the p_x and p_y bands, but the crossing will remain (Fig. 8b). The shifts along the a direction, resulting in dimer formation, will pull down the bonding $p_x\sigma\pi$ and $p_x\rho\pi^*$ states and push up the antibonding $p_x\sigma^*\pi$ and $p_x\sigma^*\pi^*$ ones, thus leading to an energy gain and a gap opening along Γ–X (Fig. 8c). Along Γ–Y the crossing of the $p_y\sigma\pi^*$ and $p_y\sigma^*\pi$ bands still remains. Now we use a localized picture and grasp the role of the additional P6 sites in $GdCuP_{2.20}$. If the p_x orbitals of P5 form bonds in the dimers, the half-occupied p_y orbitals of P5 are not much involved in the bonding. When P6 is introduced into the structure, its atomic orbitals will interact with the p_y orbitals of P5. To see the energy gain MOs are constructed from the $\sigma\pi$, $\sigma\pi^*$, $\sigma^*\pi$, and $\sigma^*\pi^*$ combinations of the P5 p_y orbitals and the P6 s and p orbitals. At the Γ point the symmetry-allowed overlaps are only those between $p_y\sigma\pi$ and s and p_z, $p_y\sigma\pi^*$ and p_x, $p_y\sigma^*\pi$ orbitals of P5 and p_y orbitals of P6 (Fig. 9). As a consequence of bond formation, the resulting bonding MOs have lower energies than the original orbitals; the opposite is true for the antibonding MOs. The nine electrons occupy the lowest five MOs, with the HOMO being higher than the p orbitals of P6 and antibonding (Fig. 9). Filling of the antibonding HOMO with one electron is costly in energy and this is probably the reason for partial occupancy of P6. In total, the change in energy is favorable and leads to an energy gain upon formation of the bands from the described MOs. The presented process of bond formation is simplified; in reality the P6 orbitals will interact not only with the p_y but also with the s, p_x, and p_z orbitals of P5. Figure 10 shows the calculated band structure of the $[(P5)_4P6]^{4-}$ layer of $GdCuP_{2.20}$. Although there are both

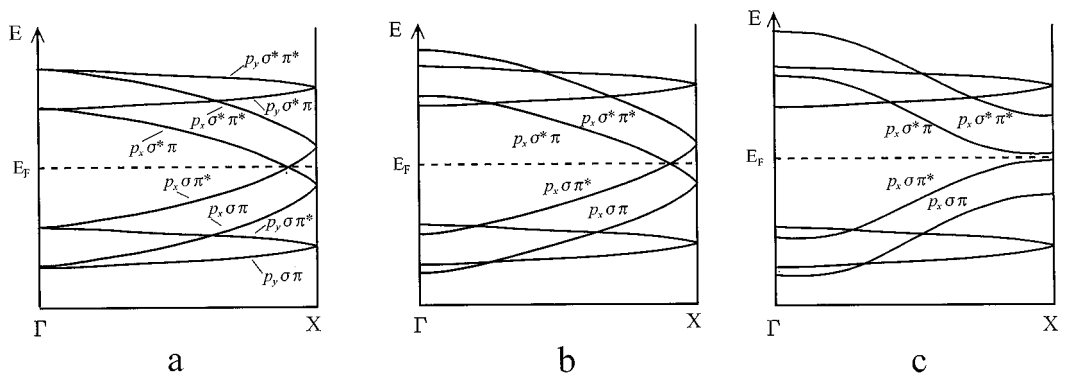

FIG. 8. Schematic band structures of the P5 layers (only p_x and p_y bands are shown) along Γ–X: (a) the P5 layer is square; (b) after an orthorhombic distortion ($a < b$) like that in $GdCuAs_{1.15}P_{0.85}$; (c) phosphorus dimers are formed. The dashed line represents the Fermi level.

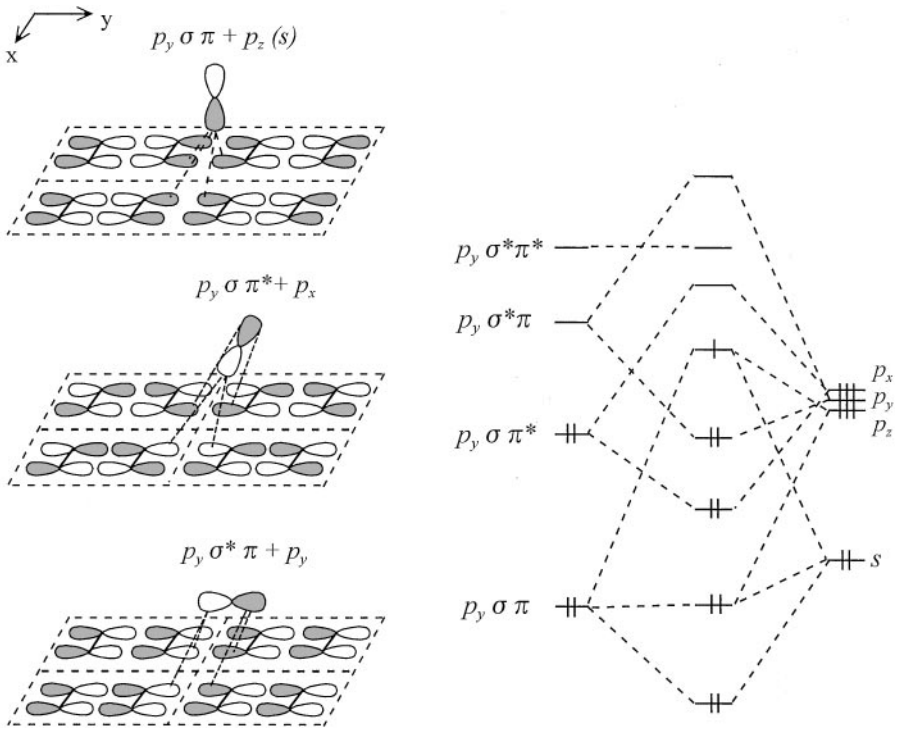

FIG. 9. MOs formed from p_y orbitals of P5 and *s* and *p* orbitals of P6 (left); schematic energy diagram of the obtained MOs (right).

s–p mixing and additional interactions, the character of the bands at the Fermi level can be now understood. The complete band structure of $GdCuP_{2.20}$ is complicated, but the bands at the Fermi level are formed mainly by the P5 and P6 orbitals and their character is similar to that of the bands in Fig. 10. The complete band structure is not presented since it does not contribute much to the further understanding of the distortion process.

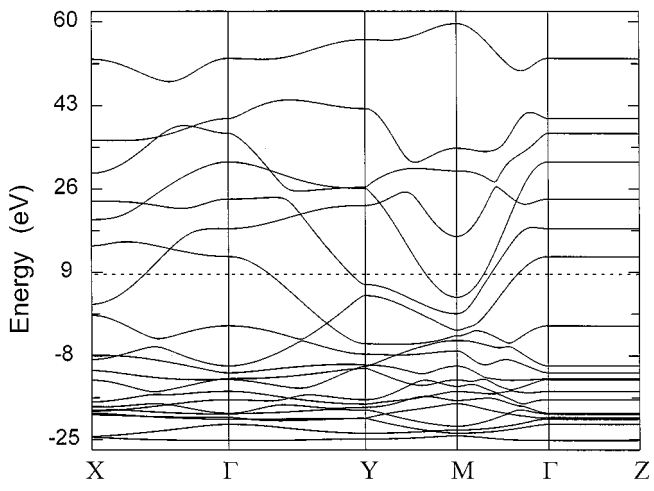

FIG. 10. Calculated band structure of the $[(P5)_4P6]^{4-}$ layer of the phosphide. The position of the Fermi level corresponds to the 78% occupancy of the P6 site.

3.4. Electronic Structure and Bonding in $GdCuAs_2$ and $GdCuAs_{1.15}P_{0.85}$

The schematic band structures in Fig. 8a and 8b also describe the As^{1-} and $(As/P)^{1-}$ layers in $GdCuAs_2$ and $GdCuAs_{1.15}P_{0.85}$, respectively. The partial DOS calculated for As^{-1} net of $GdCuAs_2$ showed that the 2D square As^{-1} net creates partially filled bands at the Fermi level. The Fermi level is at the crossing, but no distortions, lifting the degeneracy, are observed (see also the calculated band structure of $GdCuAs_2$ in Fig. 11). One reason for this could be that the formation of the localized single bonds from delocalized ones in the square net is energetically more favorable for P than for As. The enthalpies for dissociation of the P–P and As–As single bonds can serve as qualitative (but crude) indicators of the process. They can be calculated from the enthalpies of the reactions $\frac{1}{4}\,X_4(g) = \frac{1}{2}\,X_2(g)$ and $\frac{1}{2}\,X_2(g) = X(g)$ in the gaseous form (43):

$$\tfrac{1}{4}\,P_4(g) = P(g) \quad \Delta H^\circ = 72.1(2)\ \text{kcal/mol}$$

$$\tfrac{1}{4}\,As_4(g) = As(g) \quad \Delta H^\circ = 62.0(18)\ \text{kcal/mol}.$$

The other reason may be the same as for the serie of P, As, Sb, and Bi with a decreasing magnitude of distortion (14). If so, the *s–p* mixing contributes to a large distortion in $GdCuP_{2.20}$ and a lesser distortion in $GdCuAs_{1.15}P_{0.85}$ and has no effect in $GdCuAs_2$.

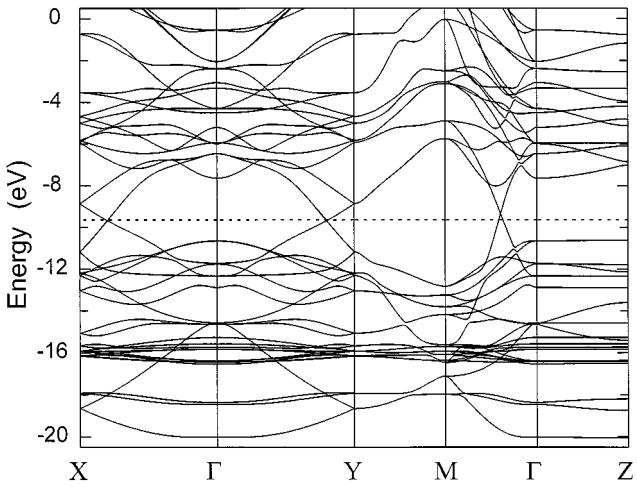

FIG. 11. Band structure of $GdCuAs_2$.

A discussion of the partial As/P occupancies in the $GdCuAs_{1.15}P_{0.85}$ structure, in which arsenic dominates in the distorted X^{1-} layer while the phosphorus atoms are mainly in the $Cu_2X_2^{4-}$ block (Table 3), follows. From the geometric point of view the larger As atoms ($r = 1.25$ Å for the gray modification) will enter into the slightly distorted square X^{1-} net with closest neighbors at 2.721 Å. The smaller P atoms ($r = 1.11$ Å for the while modification) will prefer the compact $Cu_2X_2^{4-}$ layer.

The same conclusion will follow from the analysis of the band structure. Since due to the s–p mixing the states of the X^{1-} net are antibonding at the Fermi level (Fig. 12), the less electronegative element (As here) with the less disperse bands will be a better choice for the net. This stability conclusion is based on the fact that when the orbitals

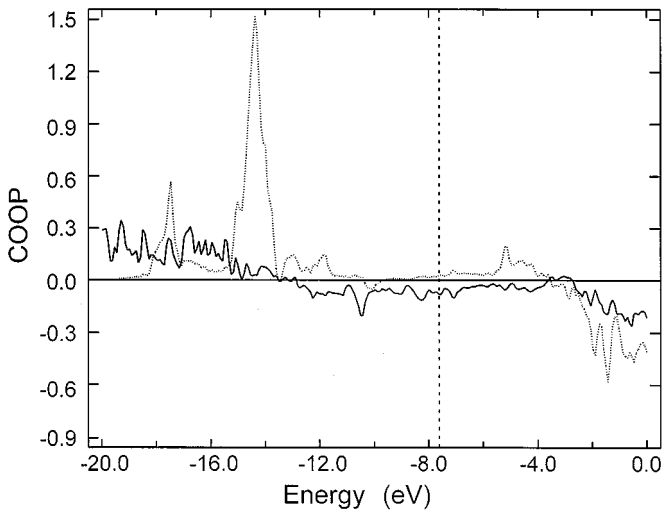

FIG. 12. COOP curves for GdCuAsP. The $X1$ and $X2$ positions are assumed to be occupied by P and As atoms, respectively. Interactions in the upper part are bonding, in the lower part antibonding. Solid line is As–As interaction, dotted line is Cu–P interaction.

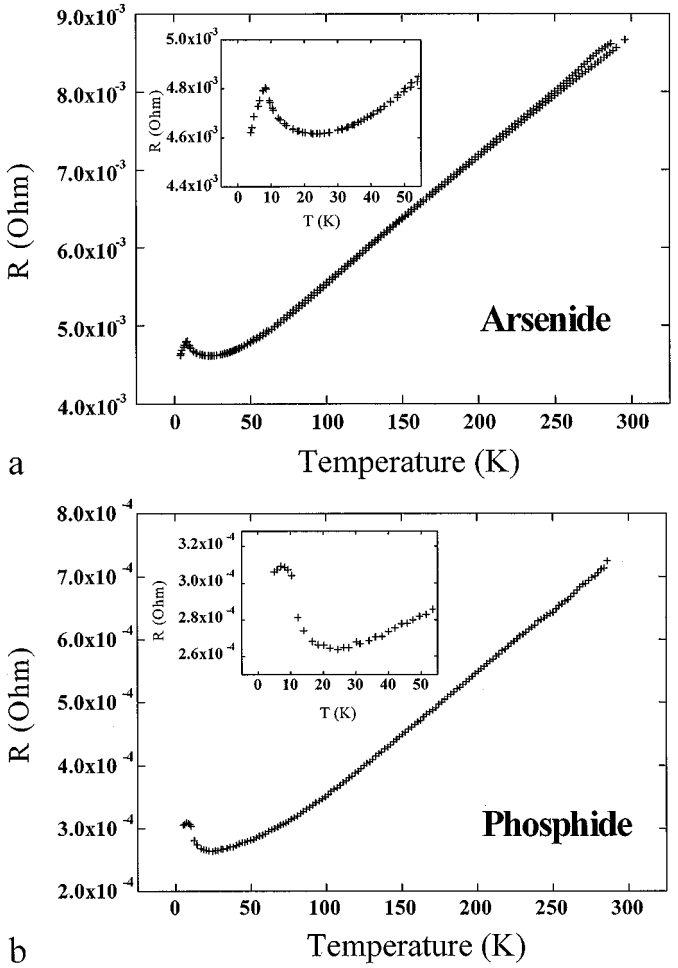

FIG. 13. Resistivity versus temperature curves for arsenide powder (a) and a phosphide single crystal (b).

overlap, the antibonding combinations are more antibonding than the bonding ones are bonding. Filling the antibonding combinations, filling the tops of widely dispersed bands, is costly in energy. However, the opposite is true for the $Cu_2X_2^{4-}$ layer. Now, the states at the Fermi level are bonding (Fig. 12) and the more electronegative element (P here) will give greater stabilization energy.

If both the geometric and energetic factors favor separation of the P and As atoms in the $GdCuAs_{1.15}P_{0.85}$ structure, the question may be asked of why the As/P mixtures exist at all. The answer comes from the entropy part in the Gibbs free energy. According to statistical mechanics the entropy for the completely random solid solution would be

$$\Delta S/R = -2(x_{As}\ln x_{As} + x_P \ln x_P) = 1.36,$$

which yields a stabilizing contribution of $1.36 \times 1073 \times 8.314 = 12{,}132$ J/mol to the Gibbs free energy at 1073 K, the temperature of the cold zone.

3.5. Electrical Conductivity and Magnetic Susceptibility

From the band structure calculations $GdCuAs_2$ and $GdCuP_{2.20}$ are expected to be metallic. Two-probe resistivity measurements reveal that the arsenide and phosphide show metallic behavior throughout the temperature range 4–285 K (Fig. 13). The specific resistivities could not be determined since the resistivities of the contacts in the two-probe technique could not be measured exactly. The resistivities decrease monotonically by about 50% for arsenide and 60% for phosphide to 4 K. Small resistivity anomalies are observed in the temperature range of the antiferromagnetic ordering; the temperatures of the resistivity increase, detected in the cooling and heating cycles, agree well with the magnetic data. No hysteresis was observed. The anomalies are typically attributed to increased spin–flip scattering in the critical temperature range.

The temperature dependencies of the inverse molar magnetic susceptibility of $GdCuAs_2$ and the phosphide are presented in Figs. 14a and 14b, respectively. The composition of the phosphide is not given since it may be different for powder and a single crystal. For both compounds the susceptibility above 50 K follows the Curie–Weiss (CW) law well. The CW parameters found by a least-squares fitting procedure are as follows: $\theta_p = -1$ K, $\mu_{\text{eff}} = 7.74\ \mu_B$ and $\theta_p = -5$ K, $\mu_{\text{eff}} = 7.87\ \mu_B$ for the powder and single crystal of the phosphide and $\theta_p = -4$ K and $\mu_{\text{eff}} = 7.96\ \mu_B$ for the arsenide. It is worth noting that the experimental values of the effective magnetic moment are very close to the value expected for a free Gd^{3+} ion with the $4f^7$ electronic configuration ($g\sqrt{J(J+1)} = 7.94$). Slight deviations of χ^{-1} (T) from straight-line behavior, observed for both ternaries below 50 K, result most presumably from crystal field interactions.

As is apparent from the upper insets to Figs. 14a and 14b, showing the behavior of χ(T) at low temperatures, the arsenide and phosphide order antiferromagnetically below 9 and 13 K, respectively. An antiferromagnetic nature of the ground state in the two compounds studied is corroborated by characteristic field variations of the magnetization (see the lower insets to Figs. 14a and 14b), which exhibit metamagnetic-like transitions in a field of about 5 kOe.

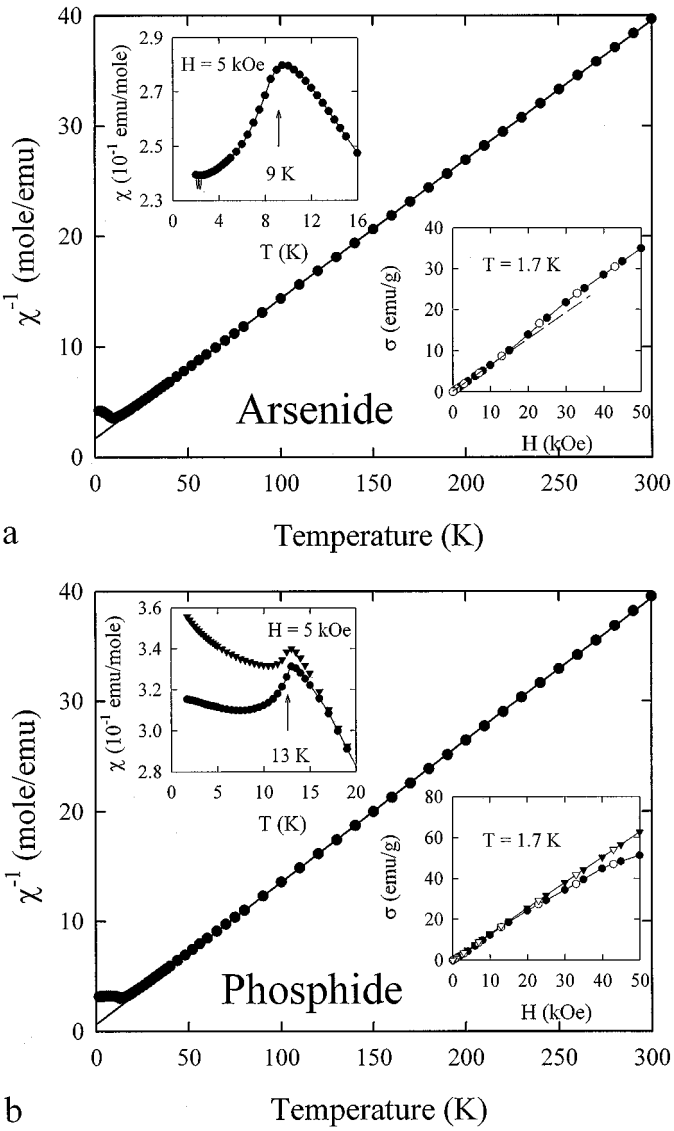

FIG. 14. Magnetic susceptibility for arsenide powder (a) and a single crystal (triangles) and powder (dots) of the phosphide (b).

4. CONCLUSIONS

The Landau theory was used for the analysis of the symmetry-breaking transitions. It showed that the transition from $GdCuAs_2$ to $GdCuAs_{1.15}P_{0.85}$ can be a continuous one; the transition from $GdCuAs_{1.15}P_{0.85}$ to $GdCuP_{2.20}$ is a first-order one. The $GdCuAs_{1.15}P_{0.85}$ structure (*Pmmn* space group) was predicted by the Landau theory.

The transitions are triggered by the innate instability of a square 2D net with partially filled bands. Only a small orthorhombic distortion is found for the (As/P) layer in $GdCuAs_{1.15}P_{0.85}$. In $GdCuP_{2.20}$ P dimers are formed along the *a* direction; these dimers are linked by the additional P atoms (P6). The additional P site has stabilizing effect on the dimers by minimizing the distortion along *b* and by preventing, in this way, the formation of the zigzag or other types of chains. Although in the $GdCuAs_{1.15}P_{0.85}$ structure both the geometric and energetic factors favor separation of the P and As atoms, the statistical As/P mixtures exist due to the entropy contribution to the Gibbs free energy.

ACKNOWLEDGMENTS

This research was supported by the Office of the Basic Energy Sciences, Materials Science Division, U.S. Department of Energy (DOE). The Ames

Laboratory is operated for DOE by Iowa State University under Contract W-7405-Eng-82. Part of the work was done at the group of Professor W. Tremel, Johannes Guttenberg University, Mainz, Germany, while Yurij Mozharivskyj was a DAAD scholar. Special thanks to Dr. Sasha Pecharsky for collecting powder diffraction data and to Dr. Dong-Kyun Seo for his help and discussion during the band structure calculations.

REFERENCES

1. R. E. Peierls, "Quantum Theory of Solids." Oxford Univ. Press, London, 1955.
2. T. A. Albright, J. K. Burdett, and M.-H. Whangbo, "Orbital Interactions in Chemistry". Wiley, New York, 1985.
3. H. A. Jahn and E. Teller, *Proc R. Soc. A* **161,** 220 (1937).
4. F. Hulliger, R. Schmelczer, and D. Schwarzenbach, *J. Solid State Chem.* **21,** 371 (1977).
5. (a)G. Sfez and C. Adolphe, *Bull. Soc. Fr. Mineral. Cristallogr.* **95,** 553 (1972); (b) R. Ceolin, N. Rodier, and P. Khodadad, *J. Less-Common Met.* **53,** 137 (1977).
6. W. Tremel and R. Hoffmann, *J. Am. Chem. Soc.* **109,** 124 (1987).
7. (a) R. Wang, R. Bodnar, and H. Steinfink, *Inorg. Chem.* **5**(8), 1468 (1966). (b) R. E. Bodnar and H. Steinfink, *Inorg. Chem.* **6**(2), 327 (1967).
8. (a) F. Hulliger and R. Schmelczer, *J. Solid State Chem.* **26,** 389 (1978); (b) M. Wittmann, W. Schmettow, D. Sommer, W. Bauhofer, and H. G. von Schnering, *in* "Solid Compounds of Transition Metals VI, International Conf., Stuttgart, 1979," p. 217.
9. (a) A. Brown and S. Rundqvist, *Acta Crystallogr.* **19,** 684 (1965); (b) D. Schiferl and C. S. Barrett, *J. Appl. Crystallogr.* **2,** 30 (1969); (c) C. S. Barrett and P. Cucka, *Acta Crystallogr.* **16,** 451 (1963); (d) C. S. Barrett and P. Cucka, *Acta Crystallogr.* **15,** 865 (1962).
10. U. Müller, "Inorganic Structural Chemistry," Wiley, Chichester, 1993.
11. J. K. Burdett and S. Lee, *J. Am. Chem. Soc.* **105,** 1079 (1983).
12. P. B. Littlewood, *J. Phys. C* **13,** 4855 (1980).
13. P. B. Littlewood, *CRC Crit. Rev. Solid State Mater. Sci.* **11,** 229 (1980).
14. D.-K. Seo and R. Hoffmann, *J. Solid State Chem.* **147,** 26 (1999).
15. E. Canadell and M.-H. Whangbo, *Chem. Rev.* **91,** 1034 (1991).
16. M.-H. Whangbo and E. Canadell, *J. Am. Chem. Soc.* **114,** 9687 (1992).
17. G. Gordier, B. Eisenmann, and H. Z. Schäfer, *Z. Anorg. Allg. Chem.* **426,** 205 (1976).
18. G. Gordier and H. Z. Schäfer, *Z. Naturforsch. B* **32,** 383 (1977).
19. E. Brechtel, G. Gordier, and H. Z. Schäfer, *Z. Naturforsch. B* **34,** 251 (1979).
20. E. Brechtel, G. Gordier, and H. Z. Schäfer, *Z. Naturforsch. B* **35,** 1 (1980).
21. G. Gordier, H. Z. Schäfer, and P. Woll, *Z. Naturforsch. B* **40,** 383 (1985).
22. O. Sologub, K. Hiebl, P. Rogl, H. Noël, and O. Bodak, *J. Alloys Compd.* **210,** 153 (1994).
23. M. Brylak, M. H. Möller, and W. Jeitschko, *J. Solid State Chem.* **115,** 305 (1995).
24. S. I. Chykhrij, Yu. B. Kuz'ma, and S. V. Oryshchyn, *Dopov. Akad. Nauk Ukr. RSR Ser. B* **3,** 63 (1989).
25. S. I. Chykhjrij, G. V. Loukashouk, S. V. Oryshchyn, and Yu. B. Kuz'ma, *J. Alloys Compd.* **248,** 224 (1997).
26. S. I. Chykhrij, Yu. B. Kuz'ma, S. V. Oryshchyn, B. V. Khabursky, and V. S. Fundamenskii, *Dopov. Akad. Nauk Ukr. RSR Ser. B* **9,** 49 (1990).
27. M. Wang, R. McDonald, and A. Mar, *J. Solid State Chem.* **147,** 140 (1999).
28. Yu. B. Kuz'ma, Yu. A. Mozharivskyj, and O. N. Panas, *Inorg. Mater.* **34,** 7 (1998).
29. Yu, Mozharivskyj, O. Lang, D. Kaczorowski, and H. F. Franzen, *presented at* the 1999 Midwest High Temperature Solid State Conference, Ames, Iowa.
30. Yu. Mozharivskyj and H. F. Franzen, *presented at* the 210th ACS National Meeting, San Franciso, California, March 26–30, 2000.
31. L. G. Akselrud, Yu. M. Grin, and P. Yu. Zavalij, CSD—Universal program package for single crystal and powder data treatment, *in* "Proc. 12th European Crystallographic Meeting, Moscow, August 20–28, 1989," *Kristallograph.* (*Suppl.*) **155,** 2 (1989).
32. "SHELXTL," Bruker Analytical X-Ray Systems, Madison, WI, 1997.
33. J. Ren, W. Liang, and M.-H. Whangbo, "Crystall and Electronic Structure Analyser (CAESAR)," North Carolina State University, Raleigh, NC, 1998.
34. S. Alvarez, "Table of Parameters for Extended Hückel Calculations," Barcelona, 1987.
35. (a) E. Hassler, T. Johnson, and S. Rundqvist, *Acta Chem. Scand. Ser. A* **27,** 123 (1974). (b) Yu. Kuz'ma and S. Chykhrij, *in* "Handbook on the Physics and Chemistry of Rare Earths" (K. A. Gscheidner, Jr., and L. R. Eyring, Eds.), Vol. 23, p. 302, Elsevier, Amsterdam, 1996.
36. H. G. von Schnering, W. Wichelhaus, and N. M. Schulze, *Z. Anorg. Allg. Chem.* **412,** 193 (1975).
37. W. Wichelhaus and H. G. von Schnering, *Z. Anorg. Allg. Chem.* **419,** 77 (1976).
38. W. Wichelhaus and H. G. von Schenergin, *Naturwissenschaften* **62,** 180 (1975).
39. L. D. Landau and E. M. Lifshitz, "Statistical Physics," Vol. 5, Pergamon, London, 1958.
40. H. F. Franzen, *Chem. Mater.* **2,** 486 (1990).
41. H. F. Franzen, "Basic Principles of Symmetry and Stability of Crystalline Solids," World Scientific, Singapore, 1994.
42. G. J. Miller, F. Li, and H. F. Franzen, *J. Am. Chem. Soc.* **115**(No. 9), 3739 (1993).
43. P. Hultgern, P. D. Desai, D. T. Hawkins, M. Gleiser, K. K. Kelley, and D. D. Wagman, "Selected Values of the Thermodynamic Properties of the Elements," *Am. Soc. Met.*, Metals Park, OH. 1973.